Flow Control Devices for Improved Enhanced Geothermal System Thermal Longevity and Power Techno-economics

Mohammad (Jabs) Aljubran[1,2], Ahmed Merzoug[3], Blake Wood[1], Koenraad Beckers[4], Mark McClure[4], Roland Horne[2]

[1]400C Energy, 35 Van Gordon St, Lakewood, CO 80228

[2] Stanford University, 450 Jane Stanford Way, Stanford, CA 94305

[3] The University of Texas at Austin, 2515 Speedway, Austin, TX 78712

[4]ResFrac Corporation, 555 Bryant St., #185 Palo Alto, CA 94301

Keywords

Flow Control Devices; Sliding Sleeves; Enhanced Geothermal Systems; Thermal Longevity; Power Generation; Techno-economics

ABSTRACT

Recent field demonstrations show that enhanced geothermal systems (EGS) have a significant potential to provide cost-competitive firm power. However, the longevity of these systems is not fully understood yet. Flow nonuniformity in EGS can cause premature thermal short-circuiting and significantly reduce system lifetime and economic performance. This study evaluated the impact of fracture flow nonuniformity using both the Gringarten analytical model and a full-physics numerical simulator calibrated with data from two EGS projects located in the United States. We introduced a passive flow control device (FCD) strategy based on sliding sleeves with engineered port sizes to mitigate flow imbalance and evaluated the lifetime system power generation potential and techno-economic feasibility. Results showed that realistic nonuniform flow conditions reduced power generation by up to 63% and increased the levelized cost of electricity (LCOE) by 45% compared to uniformly flowing systems. In modeling, we found that installing FCDs improved thermal recovery, doubled cumulative net power generation, and reduced LCOE by over 20%, even when accounting for increased pumping requirements. These findings demonstrate that passive FCDs offer a practical and scalable solution to enhance the thermal and economic sustainability of EGS development.

1. Introduction

Enhanced Geothermal Systems (EGS) have emerged as a promising approach for delivering clean firm and economic energy across diverse geologic settings (Aljubran and Horne 2024a; Augustine et al. 2023; Blackwell et al. 2011). Field demonstrations in the United States have confirmed the technical viability of EGS and its potential to produce cost-competitive electricity under favorable subsurface conditions (Aljubran and Horne 2024b; Horne et al. 2025). EGS thermal longevity

governs the system lifetime power generation potential and economic performance, and is therefore an important issue. This mandates design and technological solutions to prevent or alleviate the risk of thermal short-circuiting, i.e., early thermal breakthrough leads to premature decline in production temperature and shortened project lifetimes.

This degradation in thermal performance could be associated with flow nonuniformity across stimulated fractures, resulting from variability in fracture conductivity and stimulation effectiveness along the wellbore (Li et al. 2016). Measurements from spinner logs and flow allocation analyses in recent field projects have revealed various degrees of flow nonuniformity across fracture clusters and stages (Utah FORGE, 2024a,b; Norbeck and Latimer 2023). These disparities can concentrate flow through a subset of fractures, thereby reducing heat sweep efficiency and accelerating thermal depletion in localized zones. Repurposed from oil and gas applications, flow control devices (FCDs) offer a mature and compelling solution to address this challenge (Hu et al. 2025). The effectiveness of FCDs has been validated conceptually for high-temperature geothermal applications, but their techno-economic value remains underexplored.

This study investigated the impact of flow nonuniformity on thermal longevity and economic performance in EGS. We combined analytical modeling using the Gringarten (1975) thermal solution with a full-physics numerical simulator (McClure et al., 2025) to assess EGS lifetime techno-economics with and without FCDs. Two EGS projects, located in the United States, were analyzed using real field data. Additionally, synthetic scenarios were constructed to evaluate the sensitivity of thermal recovery and lifetime economics to varying degrees of nonuniformity. Using off-design binary power plants developed and integrated into the Flexible Geothermal Economics Model (FGEM) (Aljubran and Horne 2024c; 2025), we captured lifetime variations in thermal efficiency with respect to the degrading production temperatures and flow rates.

2. Methodology

We used the Gringarten analytical solution (Gringarten et al. 1975) and an integrated hydraulic fracturing simulator (McClure et al. 2025) to study the effect of flow nonuniformity on the thermal longevity of EGS. We also investigated the effectiveness of FCDs in extending EGS thermal longevity for power generation and improving lifecycle economics, again using FGEM (Aljubran and Horne 2024c). We used real field data based on two projects located in the United States.

2.1 Gringarten Solution

This analytical solution represents the reservoir as an infinite set of uniformly spaced, planar fractures with fixed geometries, following a linear conceptual framework. Because the solution emphasizes fracture-dominated flow and heat transfer, it is particularly suited for EGS applications. Heat is transported by one-dimensional water flow and thermal advection within the fractures, while conduction occurs through the surrounding rock, which is assumed to be homogeneous, isotropic, and impermeable. The thermal behavior of both rock and fluid is governed by equations formulated in the Laplace domain which are then inverted numerically to obtain time-domain solutions using the Stehfest (1970) algorithm. The fracture length and height are assumed to be the well spacing and the reservoir thickness. The reservoir is assumed to be homogeneous with constant properties and with no leakoff. The dimensionless equation is solved using the Laplace form, seen in Eqs. (1, (2, and (3. We solved this equation in Laplace space using the GEOPHIRES v2.0 implementation in Python (Beckers and McCabe 2019).

$$T_{wD} = \frac{T_{r_0} - T_w(z,t)}{T_{r_0} - T_{w_0}} \tag{1}$$

$$\tilde{T}_{wD}(s) = \frac{1}{s}\exp\left(-s^{\frac{1}{2}}\tanh\frac{\rho_w c_w Q x_{eD}}{2k_r H}s^{\frac{1}{2}}\right) \tag{2}$$

$$x_{eD} = \frac{\rho_w c_w}{k_r}\frac{Q}{z} \tag{3}$$

where $T_w(z,t)$ is water temperature at the outlet z and time t, T_{r_0} is the initial temperature of the reservoir rock, T_{w_0} is the inlet water temperature, s is the Laplace variable, ρ_w water density, c_w is water heat capacity, Q is the height-normalized flow rate, k_r is the rock thermal conductivity, H is the fracture height (also, reservoir thickness), z is well spacing, and x_{eD} is the dimensionless fracture spacing.

Note that this approach assumes equal flow for all fractures. To capture flow nonuniformity, we introduced a slight modification where we solved the equation for each fracture individually, such that the aggregate production temperature was the mass-weighted average of the individual fracture outlet temperatures. We assumed the absence of thermal interference between fractures. Depending on the distribution of hydraulic conductivity across fractures, this assumption could overestimate production thermal decline over time. Nevertheless, the approach still provides a computationally efficient and reasonable approximation to analyze how thermal decline varies under various levels of nonuniformity across fractures.

2.2 Numerical Simulator

We used a full-physics, three-dimensional numerical simulator with capabilities to model hydraulic fracturing, reservoir flow, flow in the wellbore, and reservoir geomechanics (McClure et al. 2025). To represent nonuniformity, we used pre-existing fractures with no proppant and assumed no poroelastic or thermoelastic stresses. Whereas fracture hydraulic conductivity was constant, fracture aperture was allowed to change as a function of effective normal stress, assuming a mechanically closed fracture element, defined using the Willis-Richards model as seen in Eq. (4 (Willis-Richards et al. 1996).

$$E = \frac{E_0}{1 + \frac{9(\sigma_n - P)}{\sigma_{n_{ref}}}} + E_{res} \tag{4}$$

where E is the overall fracture aperture, E_0 is the aperture component due to fracture roughness, E_{res} is the irreducible minimum aperture, P is pore pressure, σ_n is normal stress, and $\sigma_{n_{ref}}$ is the effective normal stress at which E reaches 10% of its maximum allowable value. We used E_0, E_{res}, and $\sigma_{n_{ref}}$ values of 0.003947 ft, 0.000004 ft, and 10,000 psi, respectively.

2.3 EGS Configuration Based on Field Data

We configured a base case of an EGS design using field data following McClure et al. (2024). This base configuration was fixed across models in this study as we were interested in investigating the

effect of nonuniformity on recovery in real settings, rather than history matching field data. We matched flow per cluster/stage as reported in two real projects: Project A (Moore et al. 2019; Utah FORGE 2024; England 2024; Utah FORGE, 2024a,b; England et al. 2025) and Project B (Norbeck and Latimer 2023). History-matched fracture conductivities ranged over 0-2,352 md-ft (median of 90.9 md-ft) and 9-862 md-ft (median of 227.7 md-ft) in Project A and Project B, respectively.

Figure 1 and Figure 2 summarize flow rate distribution per cluster and per stage for Project A and Project B, respectively. Whereas no flow measurements were taken for the bottommost four clusters in Project A, we assumed they had equal flow rate. As the Project B data were only available per stage (rather than per cluster), we assumed uniform flow across clusters per stage, such that flow only varied from one stage to another. In both projects, we also assumed that clusters were fully connected between the injector and producer. We followed an iterative approach to history match flow per cluster/stage. We first assumed constant conductivity across clusters/stages, then iteratively adjusted conductivity per cluster/stage to match the corresponding measured flow rate. This required three to five iterations on average. In the numerical simulator, Project A was modeled fully considering all 27 clusters while Project B was configured as a sector model where the 16 stages were represented as six equivalent clusters using a flow scaler.

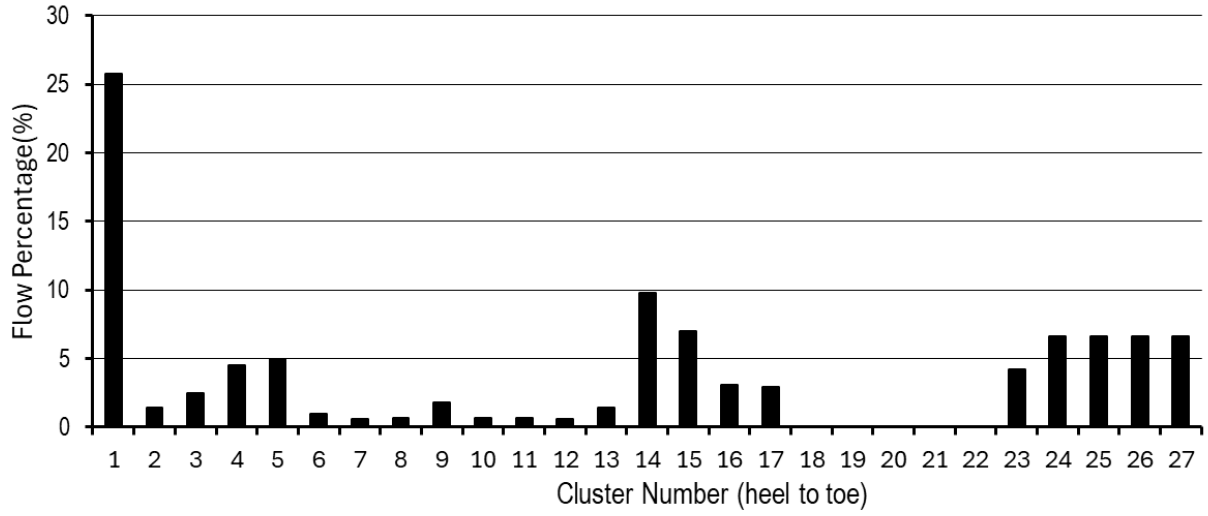

Figure 1: Flow distribution per cluster in Project A (Moore et al. 2019; Utah FORGE 2024; England 2024; Utah FORGE, 2024a,b; England et al. 2025).

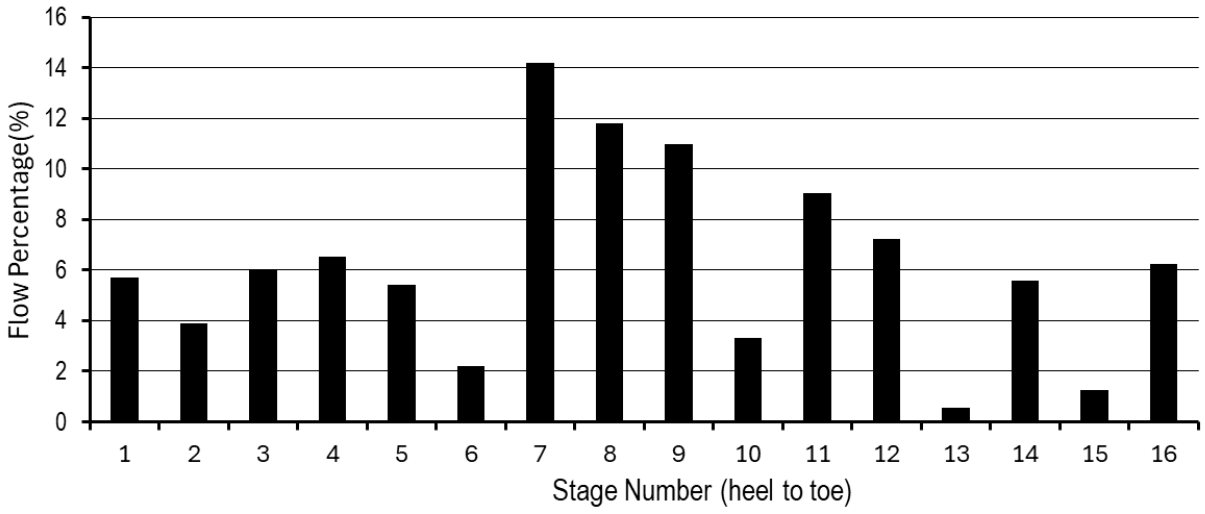

Figure 2: Flow distribution per stage in Project B (Norbeck and Latimer 2023).

In addition to the history-matched configurations of Project A and Project B, we created synthetic scenarios with various flow distributions (i.e., fracture conductivity distributions) and fracture locations to understand the effect of nonuniformity on the system performance. Fracture conductivity was set based on a log-normal distribution while fracture locations were assigned either randomly or such that highly conductive fractures were adjacent to one another.

Additionally, we simulated the effect of installing FCDs along the wellbore. Specifically, we considered a sliding sleeve stimulation technology integrated with an engineered port to constrict flow per fracture. This stimulation approach involves specialized stimulation joints that are connected to and run with the production casing along the lateral section. Each sliding sleeve joint incorporates ball-activated seat profiles, such that the largest and smallest seat profiles are located at the topmost and bottommost joints, respectively. Graduated balls are then dropped downhole in sequence to activate each sliding sleeve. Upon activating each sleeve and establishing access to the corresponding reservoir section, pressure is applied hydraulically from surface to fracture the rock. In the numerical simulator, these flow ports were simulated by considering smaller perforation diameter during the production phase of simulation. Specifically, we assumed a simple design where the FCD port diameter was constant for all fractures. To evaluate sensitivity of lifetime economics to port size, we considered sizes of 0.1, 0.125, 0.15, 0.175, 0.2, and 0.25 in.

To evaluate the effect of nonuniformity with and without FCDs in Project A and Project B for power generation, we had to consider a power plant's ability to convert heat to power under thermal decline. This required the use of off-design power plant performance which we adopted from Aljubran and Horne (2025). To normalize thermal recovery, we first simulated each project under perfectly uniform flow to yield the theoretically best total recoverable thermal energy. We then simulated each project under hypothetical nonuniform flow settings with and without FCD and defined recovery factor (RF) as seen in Eq. (5.

$$RF = \frac{Energy_{Nonuniform}}{Energy_{Uniform}} \tag{5}$$

Also, to characterize nonuniformity, we utilized the flow uniformity index (FUI), defined by Nagarajan et al. (2022), seen in Eq. (6.

$$FUI = 1 - \frac{1}{2}\frac{\sum_{i=1}^{n}|q_i - \bar{q}|}{\sum_{i=1}^{n} q_i} \tag{6}$$

where q_i, and $\bar{q}$ are the flow at the fracture i, and the average flow per fracture, respectively. These parameterizations of RF and FUI provide means for characterizing nonuniformity and system performance for power generation.

2.4 Limitations

The numerical simulations were based on a high-level comparison with field data, not on a detailed model calibration and history match. The model was also configured with homogeneous reservoir properties, and constant fracture conductivity distribution which likely would not be the case in the field as fracture characteristics could change due to poro-thermo-elastic-chemical effects. Hence, the study results are useful to quantify the value of flow uniformity but should not be taken as literal predictions of future thermal decline at these projects. Future work could explore these system configuration specifications and poro-thermo-elastic-chemical effects in more detail.

3. Results and Discussion

3.1 Gringarten Modeling

We simulated Project A and Project B using production mass flow rates of 26 kg/s and 60 kg/s, respectively. Well spacing (also, fracture length) was set to 350 ft in Project A and 600 ft in Project B. Fracture spacing and height were set to 30ft and 600ft, respectively, in both projects. The Gringarten model was configured using input parameters seen in Table 1. Both projects were modeled once using the actual/measured flow distribution and once assuming uniform flow distribution. Results were then compared in terms of the practical project lifetime for power generation. Using the off-design power plant model by Aljubran and Horne (2025), we found that power generation in this EGS setting would have dropped by over 75% upon reaching 150°C production temperature. Hence, in this section, we defined performance based on the number of years before production temperature declines to 150°C.

Table 1: Gringarten model configuration and input parameters

Property	Value	Property	Value
Reservoir temperature	200°C	Water injection temperature	80°C
Rock thermal conductivity	2.5 W/m-C	Water thermal conductivity	0.6 W/m-C
Rock heat capacity	1000 J/kg-C	Water heat capacity	4184 J/kg-C
Rock density	2700 kg/m^3	Water density	1000 kg/m^3

Figure 3 shows the temperature decline of Project A modeled using the Gringarten solution for actual/measured versus uniform fracture flow distributions. Project A exhibited a relatively low FUI of 0.54, because this project was experimental and focused on testing different technologies and stimulation designs rather than optimizing system longevity and performance. Additionally, Project A field data indicated that this EGS doublet intersected a fault which could have contributed significantly to nonuniformity (McClure 2025). Results predicted that the practical Project A lifetime with the realistic nonuniform flow distribution will be only 1.2 years, i.e., more

than 50% lower than the result would have been with a uniform flow distribution. It is important to emphasize that Project A was experimental, hence the fracture flow distribution was significantly nonuniform by design, for research purposes.

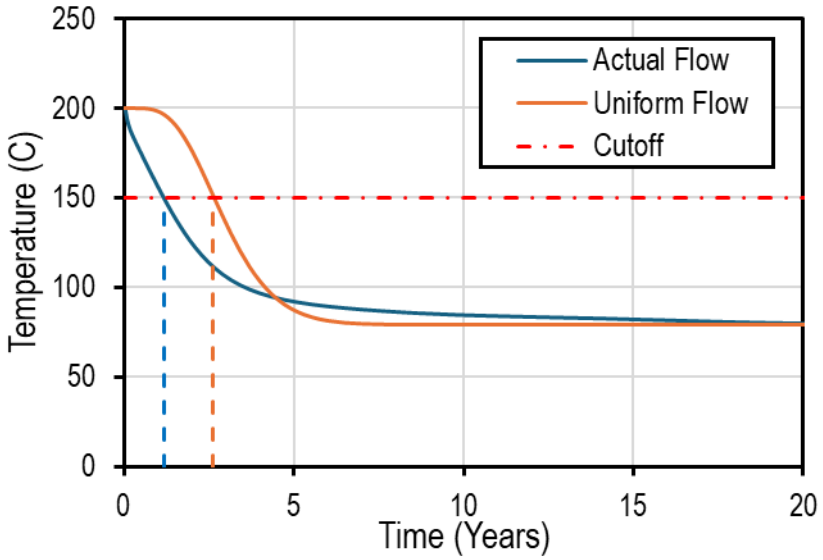

Figure 3: Temperature decline of Project A modeled using the Gringarten solution under actual/measured and uniform fracture flow distributions.

Figure 4 shows the temperature decline of Project B modeled using the Gringarten solution for actual/measured versus uniform fracture flow distributions. Project B was associated with a FUI of 0.78, estimated by comparing stage-level flow allocation. FUI could be lower if flow distribution data were available at the cluster level which would reflect greater flow variability per fracture. Due to lack of data, we assumed that clusters within each stage flowed at the same rate. This could be a source of inaccuracy, however, as different clusters within the same stage often flow at different rates. Project B was estimated to last for 5.8 years under the measured/actual flow nonuniformity, a 24% reduction compared to its uniform flow counterpart. It is important to emphasize that Project B was a pilot, not a full-scale commercial project.

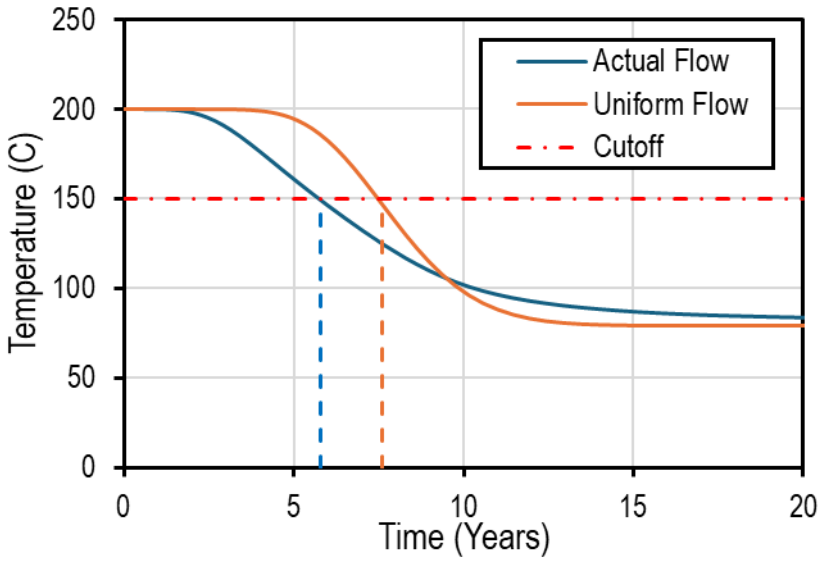

Figure 4: Temperature decline of Project B modeled using the Gringarten solution under actual/measured and uniform fracture flow distributions.

We observed a strong relationship between the FUI and practical project lifetime for power generation and RF. Considering the Project B configuration, we used the Gringarten model to simulate practical project lifetime for different values of FUI. As seen in Figure 5 and Figure 6, results are reported as time to practical project lifetime (i.e., time to hit 150°C in years) and the associated thermal recovery factor. We accurately represented these relationships using a near-linear quadratic function, which provides a useful utility to analyze thermal recovery and power generation under different flow uniformity scenarios.

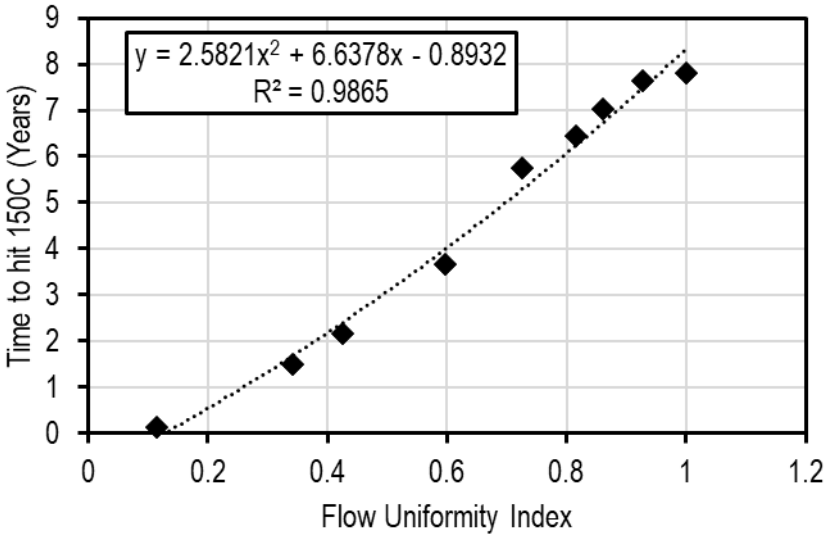

Figure 5: Empirical relationship between flow uniformity index and practical project lifetime for power generation in Project B.

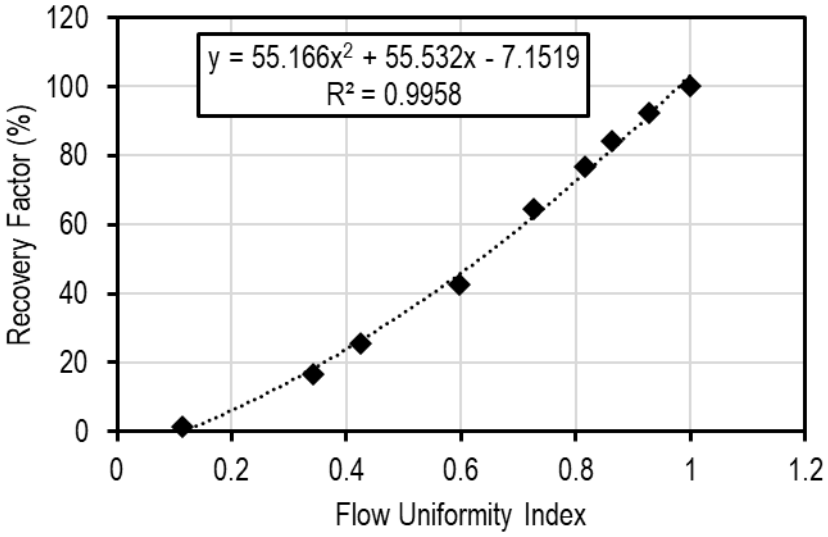

Figure 6: Empirical relationship between flow uniformity index and thermal recovery factor in Project B.

3.2 Numerical Modeling

We populated the formation properties in the numerical simulations following the EGS configuration reported by McClure et al. (2024). We then iteratively adjusted hydraulic conductivity per stage/cluster to match measured flow in Project A and Project B. We initiated all fractures at 250 md-ft and simulated flow dynamics to estimate flow per fracture. We then tuned hydraulic conductivity per fracture such that the corresponding flow resembled the measured data. We repeated these steps iteratively until a satisfactory match was achieved as seen in Figures Figure 7Figure 8. Project A was fully represented numerically with all 27 clusters, while Project B was configured as a sectorial model with 16 clusters and 1/6 flow scaler to account for the reported field design of Project B with six clusters per stage.

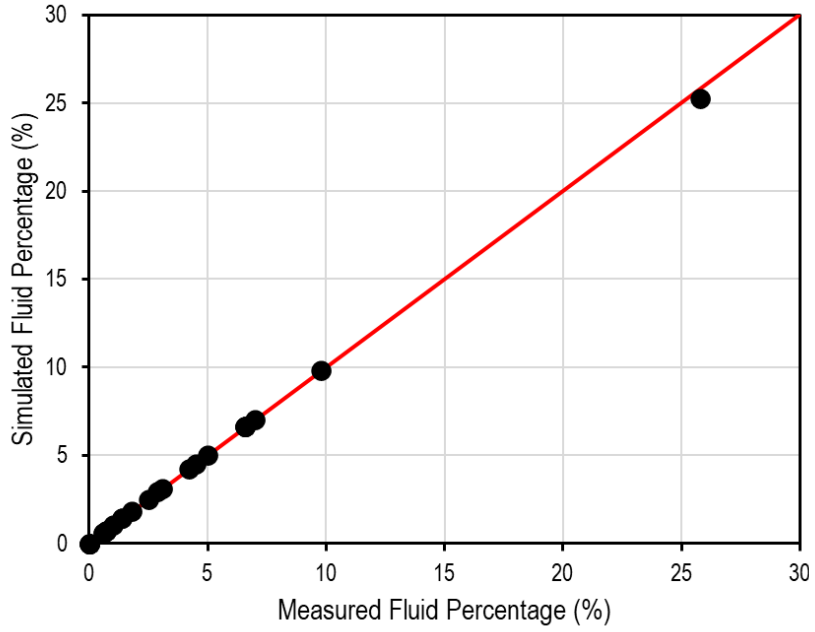

Figure 7: History match of measured flow per cluster in Project A using the numerical simulator.

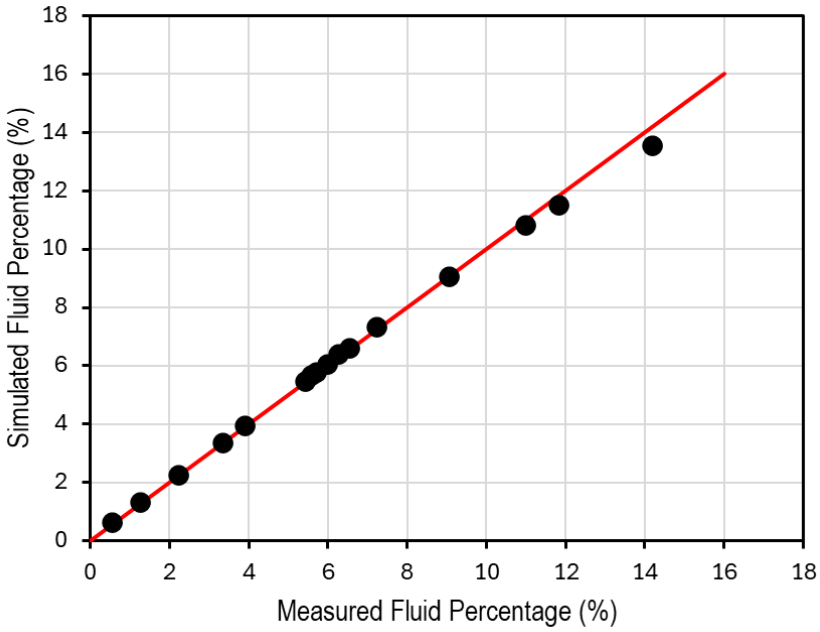

Figure 8: History match of measured flow per stage in Project B using the numerical simulator.

As seen in Figures Figure 9Figure 10, we simulated the production phase of Project A and Project B to capture temperature decline, using the full simulator model rather than the Gringarten solution. Using the 150°C lifetime cutoff once again, Project A lasted for 3 years under actual/measured fracture flow distribution, a 42% reduction compared to its fully uniform flow counterpart. Project B lasted for 5.2 years under actual/measured fracture flow distribution, a 13% reduction compared to its fully uniform flow counterpart. Overall, we noted a slower temperature decline in the numerical simulations compared to the Gringarten solution. This was attributed to

the fact that highly conductive fractures also drain heat from rock volumes around less conductive fractures. This benign thermal interference across fractures was not captured using our configuration of the Gringarten solution where we modeled each fracture separately to represent flow nonuniformity.

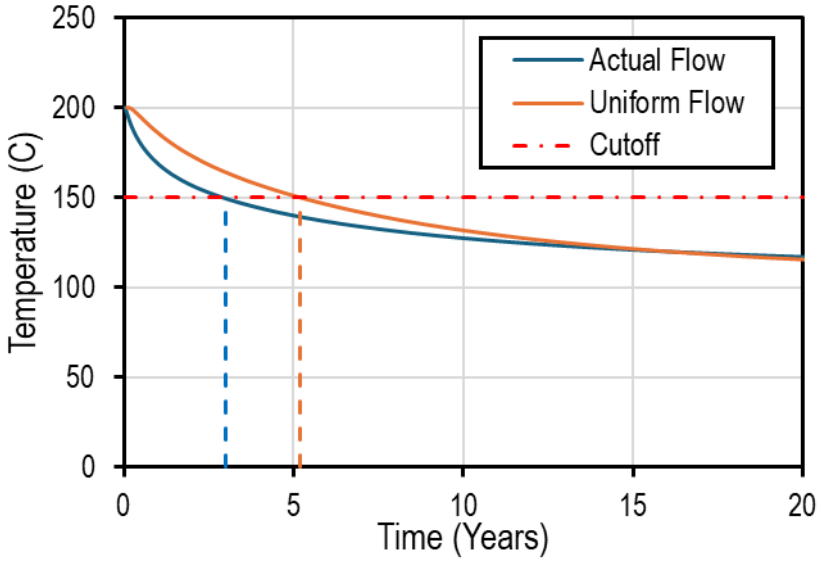

Figure 9: Temperature decline of Project A modeled using the simulator solution under actual/measured and uniform fracture flow distributions.

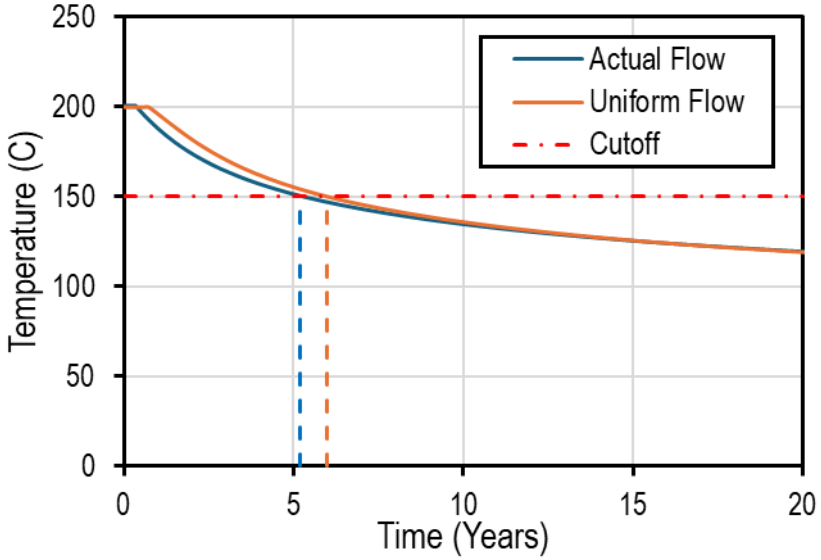

Figure 10: Temperature decline of Project B modeled using the simulator solution under actual/measured and uniform fracture flow distributions.

We also simulated synthetic cases for different values of FUI to observe how that would affect EGS performance, as seen in Figures Figure 11 and Figure 12. We assigned various hydraulic conductivities to fractures, estimated FUI, and simulated production accordingly. We followed two distributions to represent practical flow nonuniformity scenarios in terms of variability in fracture hydraulic conductivity. One method involved a bimodal distribution, such that high

conductive fractures are grouped together (Simulation B), while the other method involved a random logarithmic distribution (Simulation L). We note that the logarithmic distribution was more representative of the actual fracture distribution observed in Project B. Seen in Figures Figure 11 and Figure 12, the biomodal distribution resulted in greater temperature decline. This was attributed to the setting of highly conductive fractures near one another, yielding rapid thermal depletion of a rock volume and unfavorable heat sweep along the lateral. A bimodal distribution is likely in practice because rock heterogeneity, natural faulting/fracturing, and well undulation could favor a stimulation result where the highest conductivity fractures are close to each other.

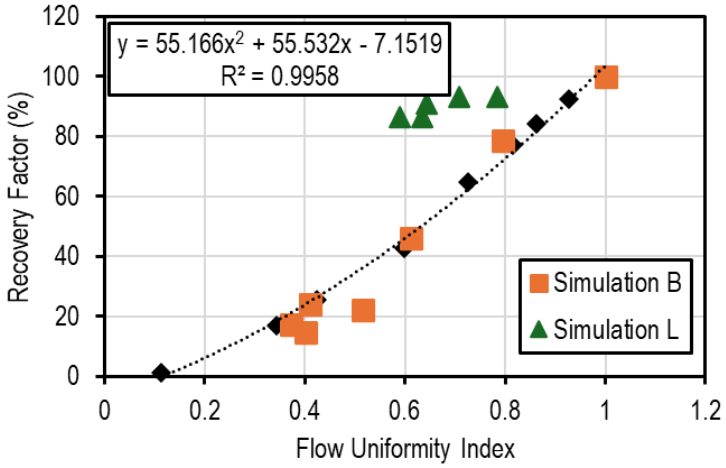

Figure 11: Plot of recovery factor versus flow uniformity using different models and configurations, namely the Gringarten solution (black), and the numerical simulator with fracture hydraulic conductivity varied following logarithmic (Simulation L) and bimodal (Simulation B) distributions.

Figure 12: Top view of temperature distribution at year 5 of production, with logarithmic (right) and bimodal (left) distributions of fracture hydraulic conductivities (Fractures are hidden for visual convenience).

3.3 Flow Control Devices and EGS Techno-Economics

We modeled the effectiveness of using FCDs as a preventive measure to alleviate flow nonuniformity. Specifically, we considered a FCD design with all-metal sliding-sleeve stimulation

technologies and engineered, plated flow ports to constrict flow per fracture. Using no elastomeric materials, this flow control approach is superhot-capable and can passively encourage flow conformance in extreme geothermal subsurface conditions. In numerical simulations, these flow ports were represented using smaller perforation diameter during the production phase of the project lifetime. Specifically, we assumed a simple design where port diameters were identical across fractures. To evaluate sensitivity of lifetime economics to port size, we considered values of 0.1, 0.125, 0.15, 0.175, 0.2, and 0.25 in.

This techno-economic analysis evaluated Project C, an EGS project configuration with parameters following those of Project B. Fracture conductivities ranged in 0.9-1,912 md-ft with median of 90.4 md-ft, following a distribution like Project B. We considered different simulation configurations with and without FCD ports. Additionally, we evaluated a scenario where fracture conductivities were perfectly uniform with 250 md-ft. Each well was equipped with a 7-inch liner installed on a 9.625-inch casing string. Numerical simulations were coupled with FGEM to evaluate lifetime power generation and techno-economic performance.

Table 2: Project C EGS system configuration.

Surface and Subsurface Characteristics			
Reservoir temperature	300°C	Vertical depth	13,250 ft
Lateral length	7500 ft	Number of fractures	250
Fracture length/height	600 ft	Fracture spacing	30 ft
System Design and Operations			
Power plant	500MWe ORC	Number of wells	32
Maximum injection pressure	2,500 psi	Target mass flow rate	100 kg/s
Casing outer/inner diameter	9.625/8.835 inch	Liner outer/inner diameter	7.000/6.184 inch
Economic Parameters			
Project lifetime	30 years	Discount factor	7%
Drilling cost	1,200 USD/meter	Stimulation cost per well	2.5 million USD
Contingency	15%	Tax credits	None

We first evaluated performance in terms of cumulative net power generation (i.e., gross power generation minus parasitic losses) for a single EGS well per scenario. Note that Project C was assumed to operate following a practical power purchase agreement requiring annual power output with >85% capacity factor. Hence, net generation was only considered for periods where an EGS well pair could deliver at >85% of its initial power generation potential (i.e., installed nameplate capacity). At times of project lifetime where capacity factor degraded below 85%, redrilling would be required to meet the contractual power offtake structure. As seen in Figure 13, the nonuniformity scenario with no FCD ports resulted in 2.81 GWhe, which was 62.6% lower than the cumulative generation of 7.52 GWhe seen under perfectly uniform flow across fractures. Installing FCD ports under nonuniform flow improves power generation to 5.23 GWhe, which was nearly 100% increase compared to the same nonuniform scenario where FCD ports were not installed. We also observed a diminishing return in power generation with respect to the FCD port size, which was attributed to the geometrically increasing frictional pressure losses with smaller port sizes, as seen in Table 3. Nevertheless, using larger FCD ports with >0.15 inch yielded over 50% increase in cumulative net power generation while only inducing marginal average pressure drop across ports.

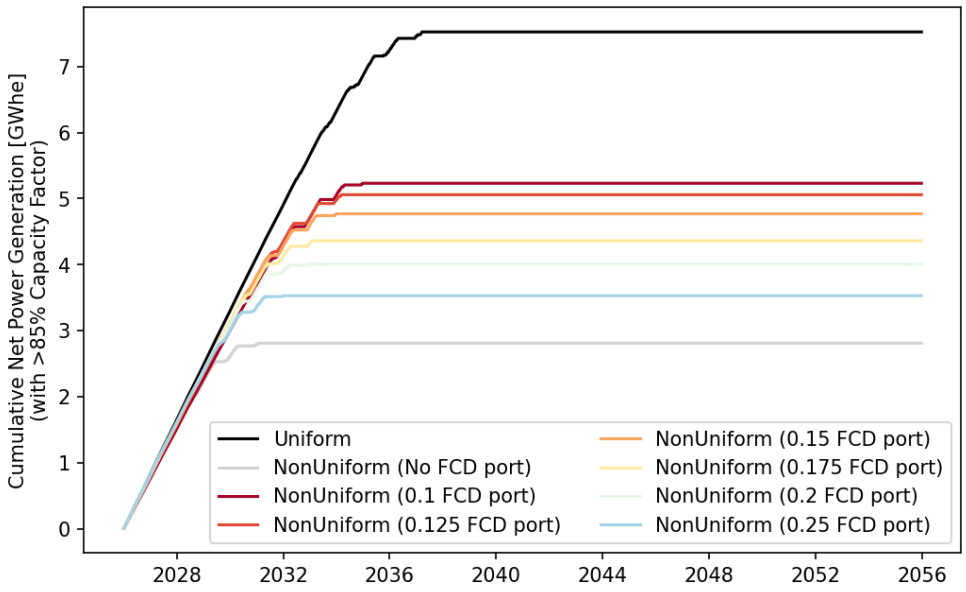

Figure 13: Cumulative net power generation for a Project C EGS well pair, following Project C design configuration, and considering different scenarios of flow uniformity and control devices.

Table 3: Pressure loss across system components for Project C scenarios with and without flow control ports.

Pressure Loss Component (psi)	Uniform	Nonuniform	Nonuniform with FCD Ports (inch)					
			0.100	0.125	0.150	0.175	0.200	0.250
Fracture Network	429.3	213.5	453.7	389.1	341.0	305.1	279.4	248.7
FCD Ports (Average)	118.3	129.8	1345.3	729.6	472.8	343.5	270.2	196.6
Injection Wellbore	706.3	706.3	706.3	706.3	706.3	706.3	706.3	706.3
Production Wellbore	810.5	810.5	810.5	810.5	810.5	810.5	810.5	810.5

Next, we evaluated the LCOE of a 500 MWe commercial project designed based on the Project C configuration, with 32 EGS well pairs. To maintain annual power generation at >85% capacity factor, redrilling was required. Redrilling frequency differed across scenarios as they experienced different production temperature decline. As seen in Table 4, developing Project C with perfectly uniform flow resulted in LCOE of 49.4 USD/MWhe. Nonuniformity yielded an increase in LCOE to 71.8 USD/MWhe. Installing FCD ports alleviated the impact of nonuniform flow and reduced LCOE to 57.1 USD/MWhe, a 20.4% improvement. Pumping requirements increased at various magnitudes when FCDs were installed, yet all scenarios with port sizes of <0.25 inch resulted in improved LCOE. The optimal FCD port size in this Project C configuration was found to be 0.125 inch. Figure 14 shows lifetime operational parameters of the scenario with 0.125-inch FCD port under nonuniform fracture conductivities at a weekly temporal timestep with parameters including ambient temperature, wellhead temperature, net power output, mass flow rate, and parasitic pumping requirements.

Table 4: Pumping requirements and LCOE across different Project C scenarios.

Property	Uniform	NonUniform	NonUniform with FCD Ports (inch)					
			0.100	0.125	0.150	0.175	0.200	0.250
Pumping Requirements (% of Gross Generation)	4.8%	4.7%	12.4%	8.9%	7.2%	6.4%	5.8%	5.2%
LCOE	49.4	71.8	58.8	57.1	58.9	59.3	62.5	66.6

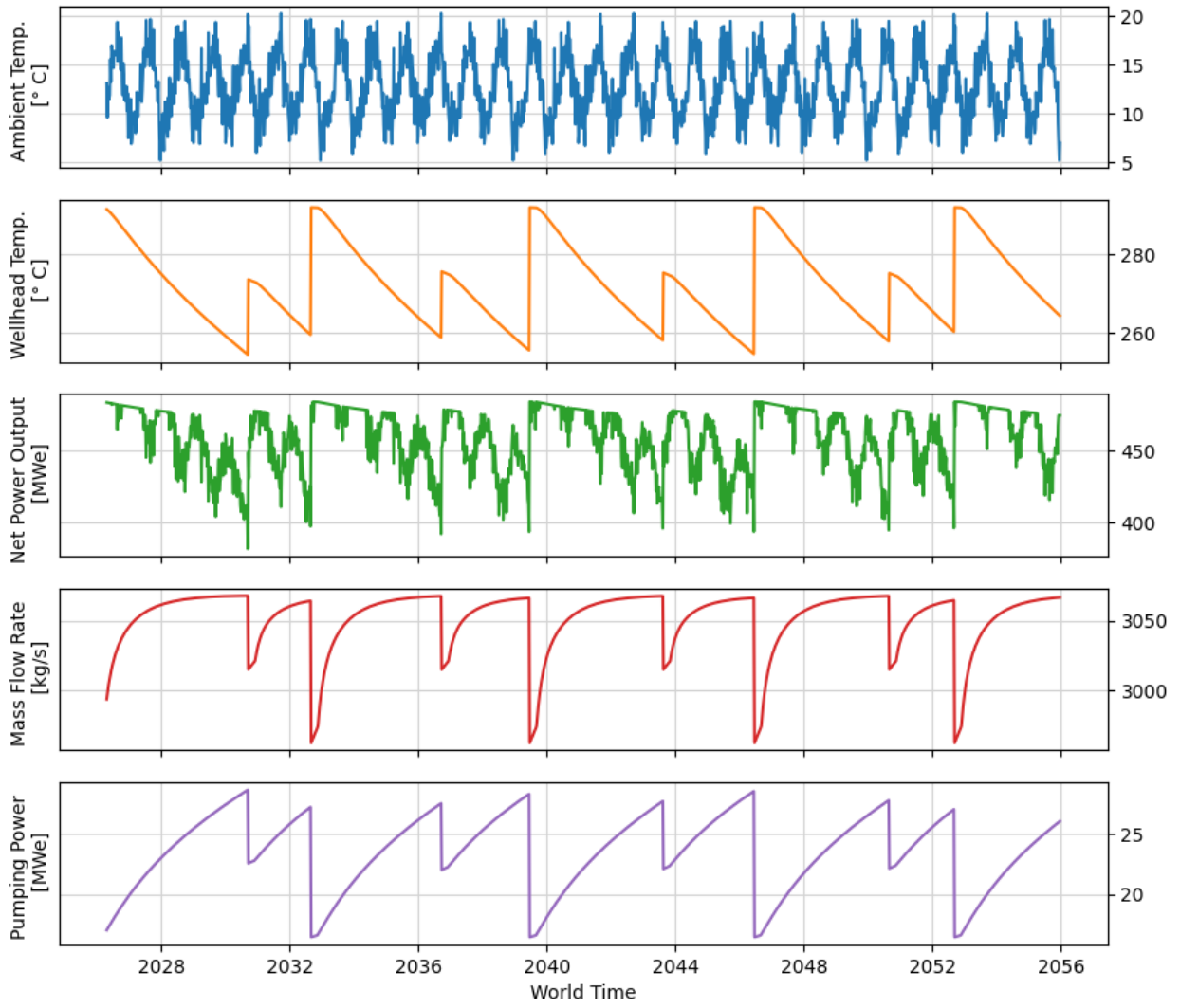

Figure 14: 30-year operational parameters of the Project C consideration under nonuniform fracture conductivities and with flow control devices installed across fractures with port size of 0.125 inch.

This study assumed no poroelastic or thermoelastic stresses, where nonuniformity is fixed and fracture geometries were not allowed to evolve during production. McLean and Espinoza (2023) found that aperture of initially highly conductivity fractures could increase by a factor of ten due to thermoelastic cooling effects, which would result in accelerated rock shrinkage and aperture increase at highly conductive fractures and significantly exacerbate short-circuiting effects and reduce heat recovery. In other words, our results only show a conservative estimate of the benefits gained from installing flow control devices. Future work could focus on modeling nonuniformity

in poroelastic or thermoelastic stresses and analyzing the added benefits effect of installing flow control devices.

4. Conclusions

This study evaluated the impact of flow nonuniformity on the thermal longevity and techno-economic performance in EGS and demonstrated the potential of passive flow control devices to alleviate thermal short-circuiting. We performed analytical modeling first using the Gringarten solution and second using numerical simulations and revealed that flow nonuniformity substantially reduced the practical project lifetime and its ability to generation power sustainably. Considering fracture conductivity distribution based on flow data from two real EGS projects, we concluded that an EGS well-pair under realistic nonuniform flow conditions experienced 62.6% reduction and the cumulative net power and 45.3% increase in LCOE compared to an equivalent system with perfectly uniform fracture conductivities. We considered passive flow control devices to alleviate this drop in performance. Installing passive flow control devices under nonuniform flow settings resulted in 100% increase in cumulative net power generation and 20.4% reduction in LCOE. Importantly, this study assumed no poroelastic or thermoelastic stresses, where nonuniformity was fixed and fracture geometries were not allowed to evolve during production. Incorporating these effects could result in accelerated rock shrinkage and fracture aperture increase at highly conductive fractures and significantly exacerbate short-circuiting effects and reduce heat recovery. In other words, our results show a conservative estimate of the benefits gained from installing flow control devices.

Acknowledgement

The authors would like to thank the Stanford TomKat Center for funding this work through the Innovation Transfer Program.

REFERENCES

Aljubran, M. J., and Horne, R. N. “Thermal Earth Model for the Conterminous United States Using an Interpolative Physics-informed Graph Neural Network.” Geothermal Energy, 12(1), 25. (2024a).

Aljubran, M. J., and Horne, R. N. “Power Supply Characterization of Baseload and Flexible Enhanced Geothermal Systems.” Scientific reports, 14(1), 17619. (2024b).

Aljubran, M. J., and Horne, R. N. “FGEM: Flexible Geothermal Economics Modeling Tool.” Applied Energy, 353, 122125. (2024c).

Aljubran, M. J., and Horne, R. N. “Techno-Economics of Geothermal Power in the Contiguous United States under Baseload and Flexible Operations.” Renewable and Sustainable Energy Reviews, 211, 115322. (2025).

Augustine, C., Fisher, S., Ho, J., Warren, I., and Witter, E. “Enhanced Geothermal Shot Analysis for the Geothermal Technologies Office (No. NREL/TP-5700-84822).” National Renewable Energy Laboratory (NREL), Golden, CO (United States). (2023).

Beckers, K. F., and McCabe, K. “GEOPHIRES v2. 0: Updated Geothermal Techno-Economic Simulation Tool.” Geothermal Energy, 7, 1-28. (2019).

Blackwell, D., Richards, M., Frone, Z., Ruzo, A., Dingwall, R., and Williams, M. “Temperature-At-Depth Maps For the Conterminous US and Geothermal Resource Estimates.” GRC Transactions, 35. (2011).

England, Kevin, PeiJian Li, Pengju Xing, Joseph Moore, and John McLennan. 2024 Enhanced Geothermal Hydraulic Fracturing Campaign at Utah FORGE. Paper SPE-223519-MS presented at the Hydraulic Fracturing Technology Conference and Exhibition, The Woodlands, TX. (2025).

England, Kevin. Review of the 2024 Stimulation Program at Utah FORGE. Hydraulic Fracturing Seminar Series, American Rock Mechanics Association Hydraulic Fracturing Community. https://www.youtube.com/watch?feature=shared&v=wFe0DVhcHak. (2024).

Gringarten, A. C., Witherspoon, P. A., and Ohnishi, Y. “Theory of Heat Extraction from Fractured Hot Dry Rock.” Journal of Geophysical Research, 80(8), 1120-1124. (1975).

Hu, J., Ou, Y., Zheng, S., & Sharma, M. “Performance of Flow Control Devices (FCDs) in Fractured Horizontal Wells for Enhanced Geothermal Systems (EGS).” In SPE/AAPG/SEG Unconventional Resources Technology Conference (p. D031S061R001). URTEC. (2025).

Li, T., Shiozawa, S., and McClure, M. W. “Thermal Breakthrough Calculations to Optimize Design of a Multiple-stage Enhanced Geothermal System.” Geothermics, 64, 455-465. (2016).

McClure, M. “Preliminary Analysis of Results from the Utah FORGE Project.” Proceedings, the 50th Workshop on Geothermal Reservoir Engineering, Stanford University. (2025).

McClure, M. et al. “ResFrac Technical Writeup.” arXiv preprint arXiv:1804.02092. (2025).

McClure, M. W., Irvin, R., England, K., and McLennan, J. “Numerical Modeling of Hydraulic Stimulation and Long-Term Fluid Circulation at the Utah FORGE Project.” Proceedings, the 49th Workshop on Geothermal Reservoir Engineering, Stanford University. (2024).

McLean, M. L., & Espinoza, D. N. “Thermal Destressing: Implications for Short-circuiting in Enhanced Geothermal Systems.” Renewable Energy, 202, 736-755. (2023).

Moore, J., et al. “The Utah Frontier Observatory for Research in Geothermal Energy (FORGE): an International Laboratory for Enhanced Geothermal System Technology Development.” Proceedings, the 44th workshop on geothermal reservoir engineering. Stanford University. (2019).

Nagarajan, P., Ström, H., and Sjöblom, J. “Transient Flow Uniformity Evolution in Realistic Exhaust Gas Aftertreatment Systems Using 3D-CFD.” Emission Control Science and Technology, 8(3), 154-170. (2022).

Norbeck, J. H. Latimer, T. “Commercial-scale Demonstration of a First-of-a-kind Enhanced Geothermal System.” Preprint, eartharxiv. (2023).

Stehfest, H. “Algorithm 368: Numerical Inversion of Laplace transforms [D5]”. Communications of the ACM, 13(1), 47-49. (1970).

Utah FORGE. Phase 3B Year 2 Annual Report: Enhanced Geothermal System Testing and Development at the Milford, Utah FORGE site. Prepared for the US Department of Energy, Contract DE-EE0007080. https://gdr.openei.org/submissions/1707. (2024a).

Utah FORGE. Utah FORGE: injection and production test results and reports from August 2024. Energy and Geoscience Institute at the University of Utah. https://gdr.openei.org/submissions/1668. (2024b).

Willis-Richards, J., Watanabe, K. and Takahashi, H. “Progress Toward a Stochastic Rock Mechanics Model of Engineered Geothermal Systems.” Journal of geophysical research: solid earth, 101(B8), 17481-17496. (1996).